Advanced Particle Shape Analysis in Conglomerate Reservoir From Borehole Resistivity Image*

Shiduo Yang[1], Weidong Huang[2], Chaofeng Chen[2], Isabelle Le Nir[1], Junyi Yuan[1], Shenzhuan Li[3], Heike Delius[4], and Krishna Pokhriyal[4]

Search and Discovery Article #42172 (2018)**
Posted January 15, 2018

*Adapted from the extended abstract prepared for a poster presentation at AAPG/SEG International Conference and Exhibition, London, England, October 15-18, 2017.

[1]Schlumberger, Clamart, France (syang4@slb.com)
[2]Petrochina, Xinjiang, China
[3]Schlumberger, Beijing, China
[4]Schlumberger, London, United Kingdom

Introduction

Sedimentary particle shape analysis provides fundamental information for interpretations of hydrodynamic conditions and depositional environments. The spatial distribution of sediment particles provides key information on reservoir quality evaluation. In conglomerates, the traditional particle shape analysis can only be achieved from laboratory testing on rock samples from fullbore or sidewall cores; it is not possible to accurately determine particle size in conglomerates from a conventional borehole image because of measurement physics constrains, and only the visible larger sediment particles can be identified.

The particle edge is often missed because of the partial gap of the pad image tool in a large-bit-size hole. A newly developed fullbore image reconstruction technology gives an opportunity to fill the pad gap and provide better visualization of heterogeneity and texture of conglomerates including the presence of pebbles, clasts and vugs. The particle shape and size analysis in a conglomerate can be estimated more efficiently from this reconstructed fullbore image.

We first analyze the patches on the images corresponding to high and low measurement by the morphological survey method on the reconstructed fullbore image or high-definition azimuthal fullbore images. The patches are representative of different sizes of sedimentary particles. Subsequently, the long/short axis length and size of the patches are calculated. Because of measurement physics, the axis length from the borehole image is slightly different from actual length measured on core data; and the length is verified with laboratory measurements on core data in different image resistivity background.

The roundness and sphericity of each patch are computed from geometry analysis of the image. The apparent dip of the long axis of patches is used for paleocurrent direction analysis; this is especially useful in a conglomerate because of the lack of crossbedding evidence.

This new solution was applied in conglomerate formation from different depositional environments in two wells, one drilled with water-based mud and the other drilled with oil-based mud. The depositional environments represented were fan delta, braided river and submarine fan. All of the paleocurrent direction analysis results are consistent with seismic interpretation or crossbedding analysis of sandstone in the same or offset wells. Moreover, the particle size distribution provides valuable information for the reservoir quality evaluation and was confirmed with mud logging or production testing data.

Methodology

The image texture can be quantitatively analyzed by delineating conductive and resistive heterogeneities (Delhomme, 1992). The quantitative heterogeneities are used for facies analysis, permeability estimation, and the evaluation of Archie cementation factor-*m*. The porosity can also be classified from conductive heterogeneities and dip data (Yamada et al., 2013). Alternatively, instead of the conductive heterogeneities for petrophysics, the heterogeneities resistivity patch size can be characterized.

After filling the empty stripe from pad image tool using structure and texture-based fullbore image reconstruction (Hurley and Zhang, 2011), we have designed a sediment particle analysis workflow (Figure 1), based on the reconstructed or existing fullbore image, which gives a continuous sediment particle statistics curve and cumulative representations.

The conductive and resistive patches from image texture analysis (Delhomme, 1992) can be extracted based on the measurement value of different resistivity image tools. In most cases, the resistive patch represents the sedimentary particle, such as sand, pebble cobble or other gravels. The computed particle size could be slightly different with actual size because the resistivity measurement is different from the optical visualization.

After high and low resistivity patch extraction, the following steps are implemented to compute the particle shape parameters:

Patch simplification. The extracted raw patches are based on image pixels, and may consist of irregular shapes due to data inconsistency between pads (wireline tools) or between sectors (logging-while-drilling tools). In addition, the large number of points in each patch consumes extensive computational cost. Thus, in the proposed workflow, these patches are processed by a polygon simplification method, which reduces the number of points, and extracts the essential characteristics of the patch for further analysis. The Ramer–Douglas–Peucker algorithm also known as the iterative endpoint fit algorithm (Prasad et al., 2012), was selected and applied for this simplification. An example of the polygon simplification of pebbles detected on an image is given in Figure 2. This step significantly reduces the number of points and allows for definition of a clear shape.

Patch segmentation. Although an irregular shape was simplified, two patches could be connected to each other because of the low resistivity contrast. The watershed segmentation solution is applied to separate connected patches based on gray-scale image analysis. The topological watershed transform (Couprie and Bertrand, 1997) is selected in this study by considering the grayscale image as topographic surface. The separating line (red line in Figure 3) is produced to separate the connected patches. In our samples, we found that several patches were still connected (pink circle in Figure 3), but the statistical result should be acceptable considering a large number of patches.

Long and short axes length. The "rotating calipers" method was used to compute the minimum bounding rectangle. A complexity convex hull algorithm is used to generate a convex polygon based on the patch polygon; then the minimal area (or minimum perimeter) enclosing rectangle is found, using the rotating calipers. The long and short axes are computed from this enclosing rectangle.

Long and short axes length calibration. The computed axis length should be calibrated with core data or local experimental data based on resistivity range. This step is optional because the length varying along with resistivity is very small, on the millimeter scale, and the value is comparable in the same well or the same reservoir area.

Patch size, roundness, and sphericity evaluation. The parameters related toparticle shape are computed from geometry analysis by following geological concepts including size, roundness, and sphericity:

$$\text{Area} = \frac{1}{2}|(x_1y_2 - x_2y_1) + (x_2y_3 - x_3y_2) + \cdots + (x_ny_1 - x_1y_n)| \quad \text{Equation 1}$$

where $(x_1, y_1) \ldots (x_n, y_n)$ are N vertices of the non-self-intersecting patch polygon.

For a polygonal patch, the numerical formula for computing roundness is given by

$$\text{Roundness} = \frac{\sum_0^n (r_i/\text{R})}{N} \quad \text{Equation 2}$$

Where r_i are the individual radii of the corners of a patch, N is the number of corners and R is the radius of the maximum inscribed circle. This equation is slightly different from the one proposed by Wadell (1932) with multiple largest inscribed circles.

There are many commonly used equations to compute sphericity. The following Equation 3 developed by Cox (1927) was used for sphericity computation, although Cox refers to it as "roundness" or 'circularity."

$$\text{Sphericity} = \frac{4\pi \cdot \text{Area}}{\text{Perimeter}^2} \quad \text{Equation 3}$$

Where the area is computed with Equation 1, and the perimeter of the polygon is straight forward. If the computed roundness is greater than 0.9, the patch is very close to circular in shape.

These three parameters – area, sphericity, and roundness can provide useful information on current energy and relative distance to material source, both vertically and laterally.

Paleocurrent analysis from long-axis azimuth. Most conglomerate deposits show no preferred orientation because of very rapid deposition. However, the long axis could be a useful indicator of transport mechanism if the ratio of long/short axis is high enough, and if the pebbles overlap one another in a consistent fashion, the depositional fabric can be defined as imbrication. In some cases these elongate pebbles are aligned in a direction transverse to the flow, and in others they are aligned parallel to the direction of the flow (Figure 4) (Lindholm, 1987). Elongation transverse to flow indicates fluvial deposits with a well developed fabric. Having the long axes parallel to flow is generally interpreted as evidence for the rapid transport in conglomerates associated with turbidite sequences and alluvial-flash flood deposits (Lindholm, 1987). In certain depositional environments, we assume that the only scenario developed is either transverse or parallel. It is straightforward to identify the paleocurrent direction based on regional geological setting for these two conditions.

The pebble clasts are assumed to have been deposited at the base of a channel or a surface with horizontal or lower angle. Structural dip removal should be applied to the paleocurrent direction analysis if the present structural dip is high.

With the above steps, we can compute the continuous particle shape parameter logs for geological interpretation (Figure 5).

Case Study from North Sea with Oil-based Mud Image

In our study field, the sedimentary succession comprises fan conglomerates and several fluvial sandstones with aeolian sand flat, braided plain or fluvial channel, lacustrine and lake-margin deposits (Loizou et al., 2006). There is no difficulty in identifying the fan delta conglomerates and fluvial sandstones or channels from the borehole image, but there is no detailed particle characterization for the conglomerates. We applied this new method based on the oil-based mud resistivity image to analyze the conglomerates in different intervals.

Particle-Shape Evaluation in Fan Conglomerates

From the particle shape parameter computation from the borehole resistivity image, we can clearly identify an upward fining trend in this study interval (Figure 6). There are five small cycles classified, based on long axis length and area size. For each cycle, the long axis length is more than 20mm at bottom, and it decreases to between 10 and15mm at the top. The patch size follows a similar trend, changing from 0.0003 to 0.0001m^2 in each cycle. There is no major change in roundness and sphericity which have value 0.6 and 0.55, respectively. Only at bottom of the cycle, are roundness and sphericity reduced slightly with relatively higher long axis length and larger patch size. These changing trends are matching with core data consistently; the smaller patch size, the higher oil-bearing grade of the core (Wan et al., 2017).

The length of the long axis was also compared with core scan image (Figure 7). In the core scan image, the average length of long axis is approximately 25 mm, and this is similar to the result from the borehole resistivity image in the corresponding interval. However, the roundness from the core image is rounded to well rounded, whereas the roundness extracted from the resistivity patches is approximately 0.6 with value a range of values 0 to 1. The sphericity is similar between the core scan image and computation result from borehole image, with a value of 0.55.

Paleocurrent Analysis with Long Axis Direction

The apparent dip angle and azimuth of long axis were computed, with the length of the long axis more than 50 mm, which is three times longer than the length of the short axis. Only flattened pebbles are considered as indictors of the transport mechanism. The apparent dips are converted to true line dips considering the borehole trajectory. In this study interval, the structural dip is very high, more 25^{o} based on bed boundary analysis. The structural dip removal was applied for the true dips from the above step. The center of line dip of long axis of stereonet display indicates the paleocurrent direction. The northeast upstream source direction is clearly shown in Figure 8 and consistent with regional paleogeographical models (Nichols , 2005).

Case Study from Northwest China with Water-based Mud Image

This study field is in the Junggar basin, northwest China. The sedimentary environment in the study interval is braided delta with complex lithology, including conglomerates and coarse sandstones interbedded with medium and fine sandstones (Wang et al., 2008). We have more than 100 m length of drilling core data to use in calibrating the computation result from this method.

Particle Shape Analysis in a Braided Delta

To validate particle shape parameters, one of core images was selected with clear identifiable patches (Figure 9). The length of long axis is 180 mm from the bore image patch and 160 mm from core scan image. Even though the lengths are not exactly the same, this calibration verifies that the length of long axis measured by the patch is trustworthy.

From the computation result, we found out the length of long axis is between 10mm and 20 mm; only in some short intervals are the long axes greater than 20 mmThe length of the long axis is consistent with braided delta depositional environment. From the change in the trend of the long axis and patch size, three patterns are identified: upward coarsening, upward fining and relatively constant (Figure 10):

- Upward coarsening, shown by the red line in the long axis track in Figure 10 is very common in a deltaic environment and represents the regressive depositional facies, for which the sediment supply exceeds the increase in accommodation space.
- Upward fining, shown by blue line in Figure 10, represents the channel filling and coarse or fine sandstones and is very common at top of interval. This blue pattern indicates that sediment supply is low compared to the accommodation space.
- The relatively constant long axis, shown by green line in Figure 10 indicates stable accommodation space and sediment supply.

Identification of these microfacies provides valuable information for the correlation analysis in a conglomerate environment.

Paleocurrent Analysis with Long-Axis Direction

In this braided delta environment, the lithology is very complex with conglomerates with different particle sizes, multiple grain sizes of sandstone, and different lithologies interbedded with each other. A dip vector plot with crossbedding is the traditional method for paleocurrent

direction analysis and has been confirmed in many clastic reservoirs. The paleocurrent direction from conglomerate in the study interval can be compared directly with crossbedding from sandstone in the same interval. Figure 11 shows the paleocurrent analysis in two intervals. The following conclusion can be drawn from Figure 11:

a) The paleocurrent direction based on the long-axis dip stereonet plot is from north-northwest to south-southeast and is consistent with the dip vector plot from crossbedding, although there is variation in dip vector plot over short intervals.
b) The paleocurrent direction based on long-axis dip stereonet plot is northwest to southeast and is similar to the dip vector plot from crossbedding. The high variation in the dip vector plot corresponds to the changed outline of the distribution in the stereonet display.

Discussion

Based on two case studies, we found out the particle shape parameters from borehole resistivity image are influenced by three major elements:

- The quality of gap-filled borehole resistivity images plays the key role for the final shape analysis. In some cases, especially in a large-bit-size well, the vertical stripe in the gap is very clear in the reconstructed borehole image (red rectangle in Figure 12a). The resistivity patch extraction is influenced directly by this vertical stripe. This influence could be removed by adjusting the extraction parameters during heterogeneity analysis with extra effort and detailed zonation.
- The resistivity patch extraction is also influenced by diagenesis or calcite (Figure 12b). The high-resistivity feature in the upper red rectangle could be the result of calcite cement or diagenesis; no clear patch features could be identified from borehole image, even by eye. Similarly, in resistivity feature in bottom red rectangle, the lithology is a carbonate shale; no patches should be extracted.
- The watershed segmentation is not robust enough in some cases to efficiently separate the connected patches (Figure 3).

Conclusions

After applying this new workflow for particle shape analysis in different mud environments, we observe that this solution is applicable in conglomerate reservoirs for lithology and microfacies identification and paleocurrent direction analysis.

The length of the long axis and the patch size extracted from borehole resistivity image represent the vertical particle shape change. Although there is no direct calibration with core image data, the statistical result of these two parameters can be used to compare different intervals of the same well or multiple wells.

The computed roundness from the borehole resistivity images is relatively lower than the expected result from the core image. The computation method should be improved in the future. The computed sphericityis sufficiently reliable for the particle shape analysis after core image calibration.

The paleocurrent direction determined from the long axis of resistivity patches provides an additional method to identify the deposit supply direction after comparison with the dip vector plot of crossbedding.

For the first time, this method enables paleocurrent analysis in a pure conglomerate-depositing environments.

Selected References

Couprie, M. and G. Bertrand, 1997, Topological gray-scale watershed transform: Proceedings, SPIE 3168: Vision Geometry VI, v. 136, p. 136-146.

Cox, E.A., 1927, A method for assigning numerical and percentage values to the degree of roundness of sand grains: Journal of Paleontology, v.1, p. 179-183.

Delhomme, J.P., 1992, A quantitative characterization of formation heterogeneities based on borehole image analysis: Paper T, presented at the SPWLA 33rd Annual Logging Symposium, June 14-17.

Hurley, N. F. and T. Zhang, 2011, Method to generate full-bore images using borehole images and multipoint statistics: SPE Reservoir Evaluation & Engineering, v.14/2, p. 204-214.

Lindholm, R.C., 1987, Primary grain fabric, *in* A Practical Approach to Sedimentology: Springer, Dordrecht, p. 59-64.

Loizou, N., I.J. Andrews, S.J. Stoker, et al., 2006, West of Shetland Revisited, *in* The Search for Stratigraphic Traps: Geological Society, London, Special Publications, v. 254, p. 225-245.

Nichols, G.J., 2005, Sedimentary evolution of the lower Clair Group, Devonian, West of Shetland: Climate and sediment supply controls on fluvial, aeolian and lacustrine deposition: Petroleum Geology Conference series 2005, v.6, p.957-967.

Prasad, D.K., K.H. Maylor, C. Quek, and S.Y. Cho, 2012, A novel framework for making dominant point detection methods non-parametric: Image and Vision Computing, v. 30/11, p. 843-859.

Wang, C., R. Zheng, J. Wang, et al., 2008, Sedimentary characteristics and evolution of Badaowan Formation of Lower Jurassic in northwest margin of Junggar Basin: Journal of Lithologic Reservoirs, v. 20/2, p. 38-39.

Wadell, H., 1932, Volume, shape and roundness of rock particles: Journal of Geology, v. 10, p. 443-451.

Yamada, T., D. Quesada, A. Etchecopar, I. Le Nir, et al., 2013, Revisiting porosity analysis from electrical borehole images: Integration of advanced texture and porosity analysis: Presented at the SPWLA 54th Annual Logging Symposium, New Orleans, Louisiana, June 22-26.

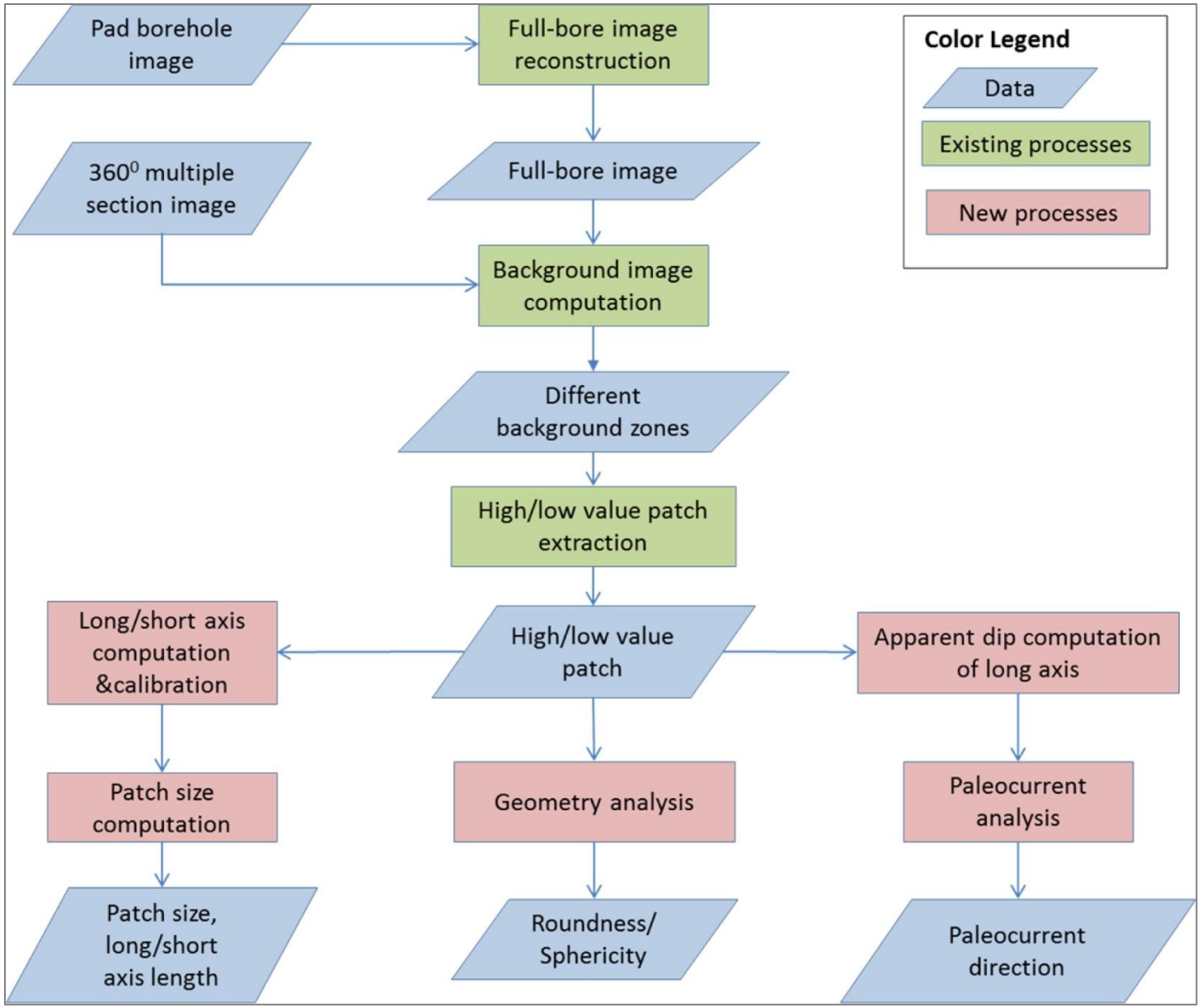

Figure 1. Workflow of sediment particle shape analysis from borehole resistivity images.

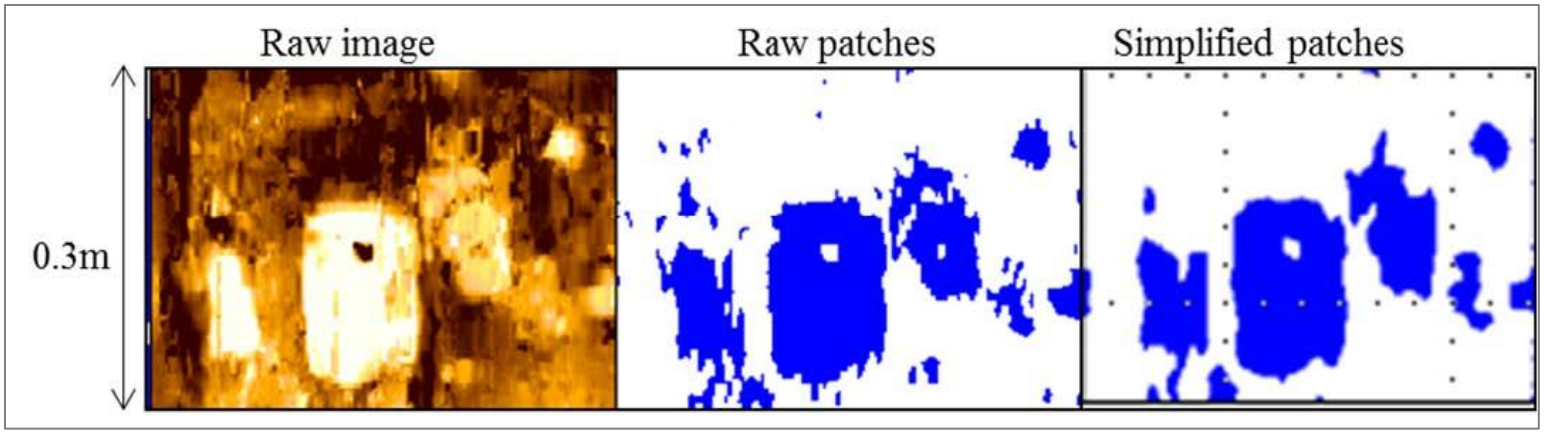

Figure 2 Simplified patches from raw resistivity image.

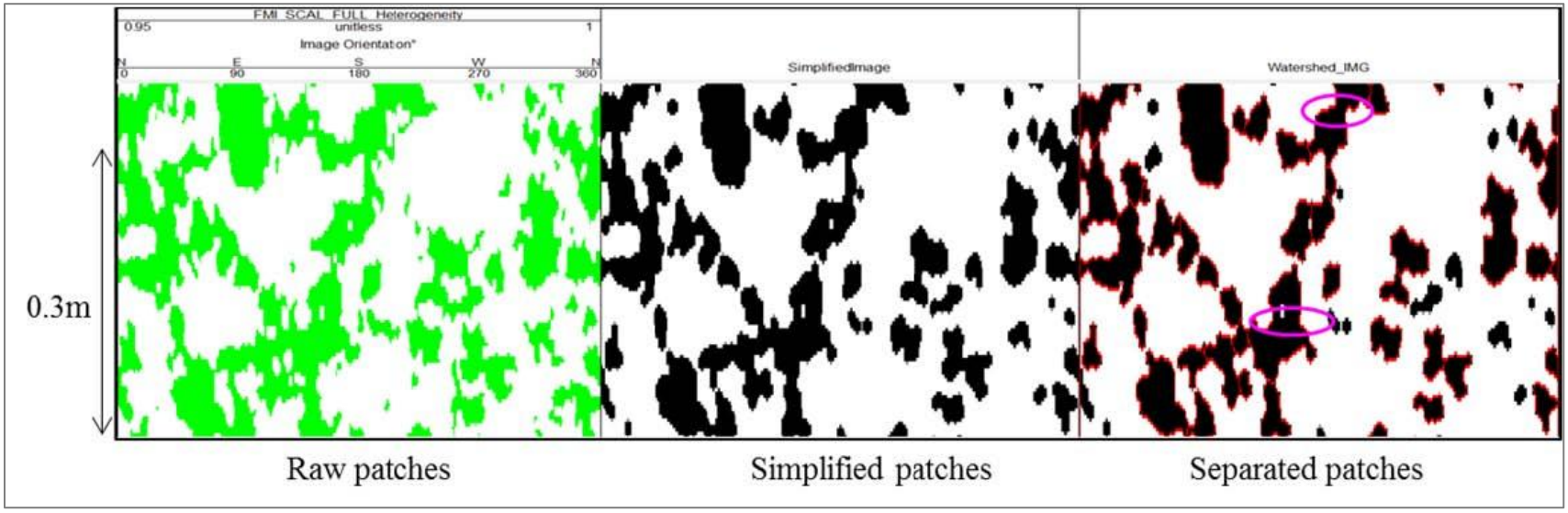

Figure 3. Separated patches from simplified image with watershed transform.

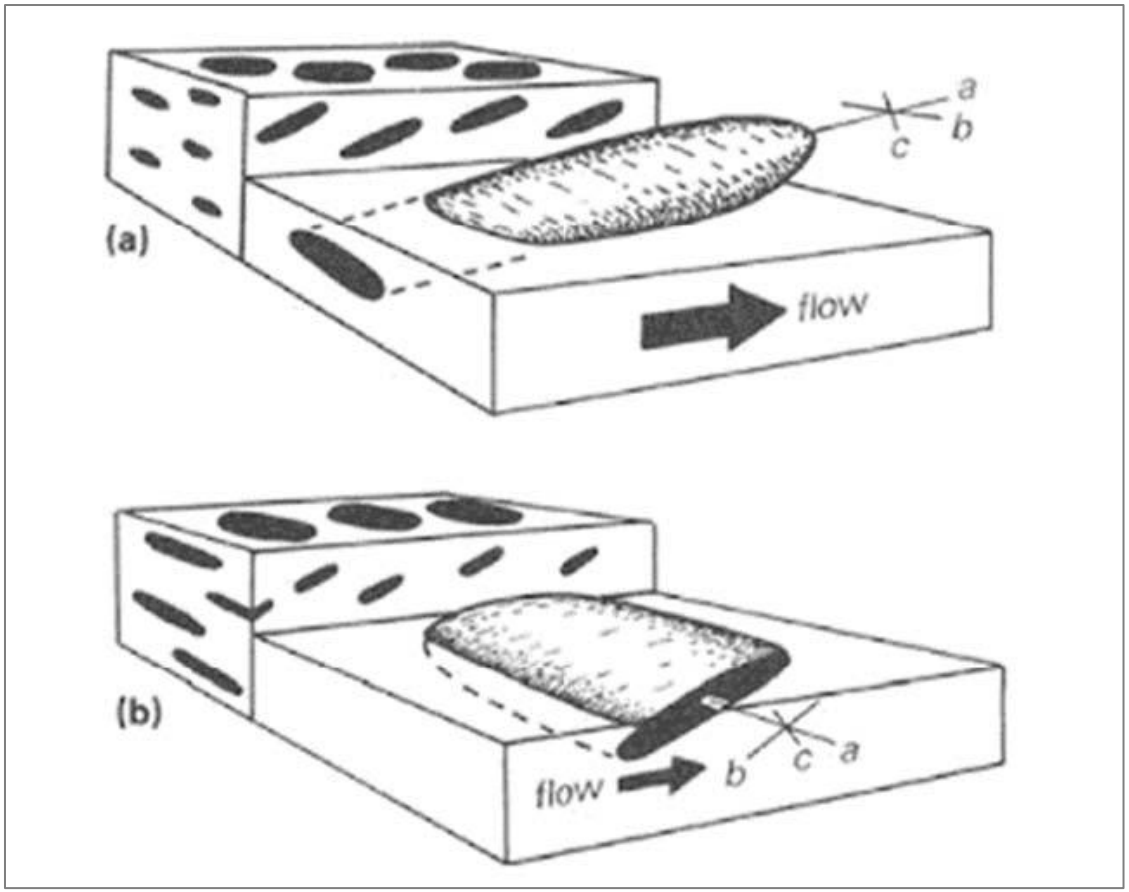

Figure 4. Pebble imbrication: (a) Long axes parallel to flow; (b) long axes transverse to flow. Reference axes follows: a, long; b, intermediate; and c, short. (From Lindholm, 1987.)

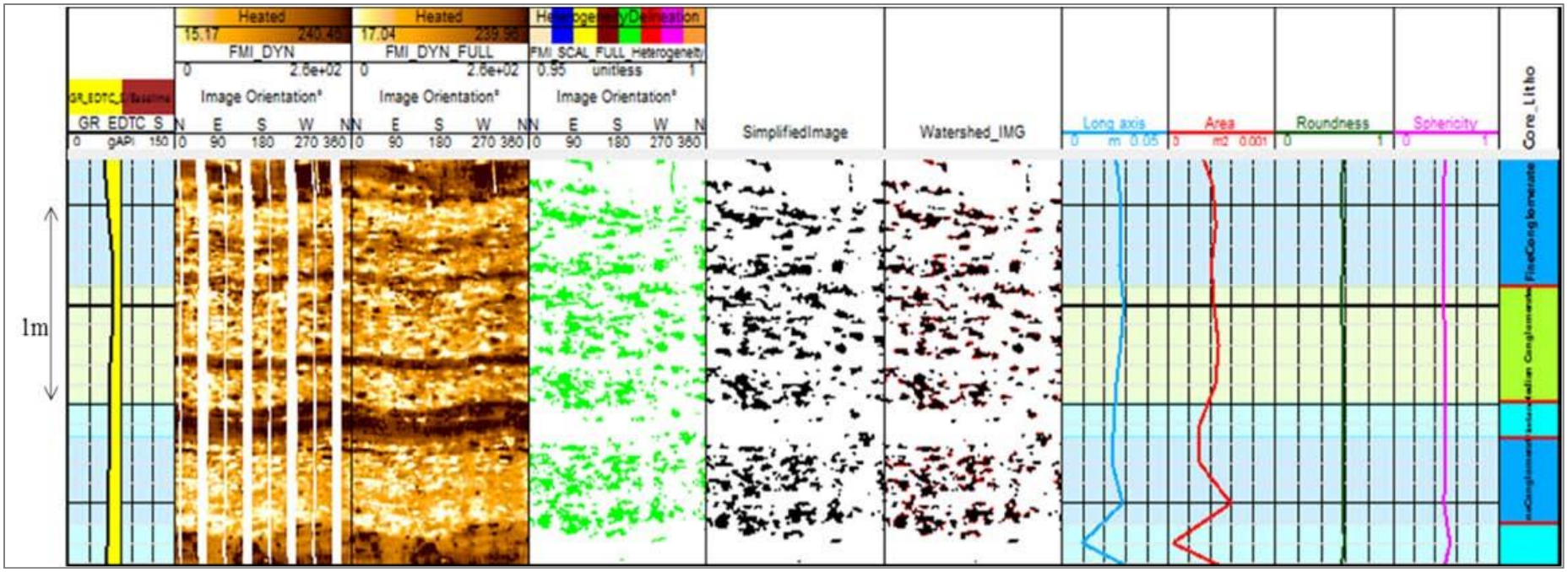

Figure 5. Particle shape analysis middle and final results. Track1, gamma ray with baseline display; track 2, dynamic borehole resistivity image with gap; track 3, gap-filled dynamic borehole resistivity image; track 4, extracted resistivity patches; track 5, simplified resistivity patches; track 6, separated resistivity patches from watershed transform; track 7, mean long axis; track 8, mean area; track 9, mean roundness; track 10, mean sphericity.

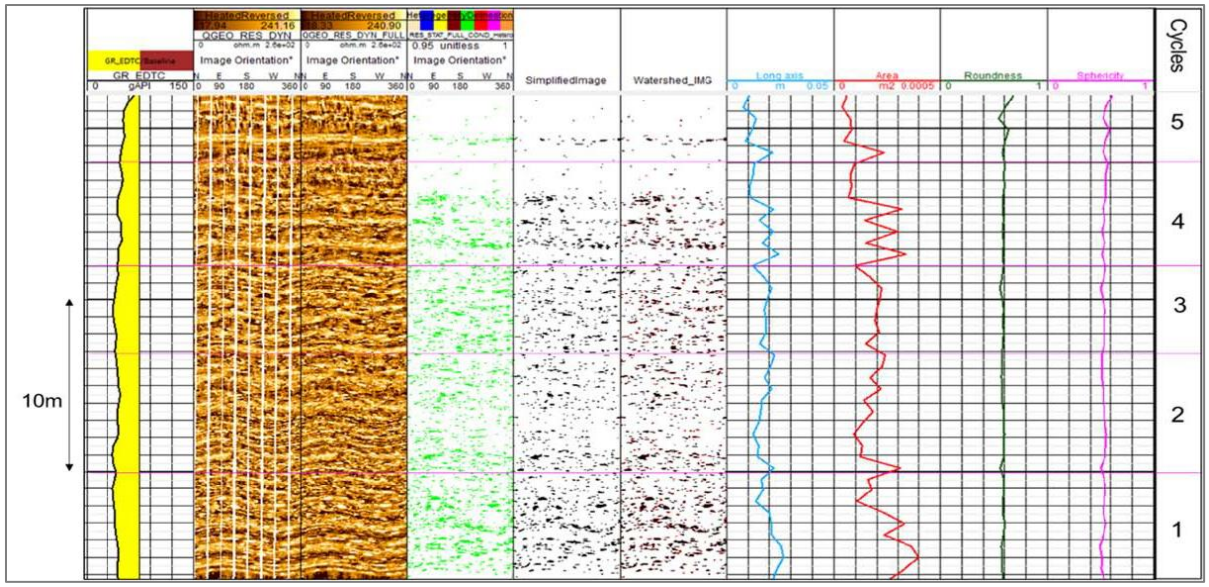

Figure 6. Cycling classification from particle shape analysis. The tracks are same as in Figure 5.

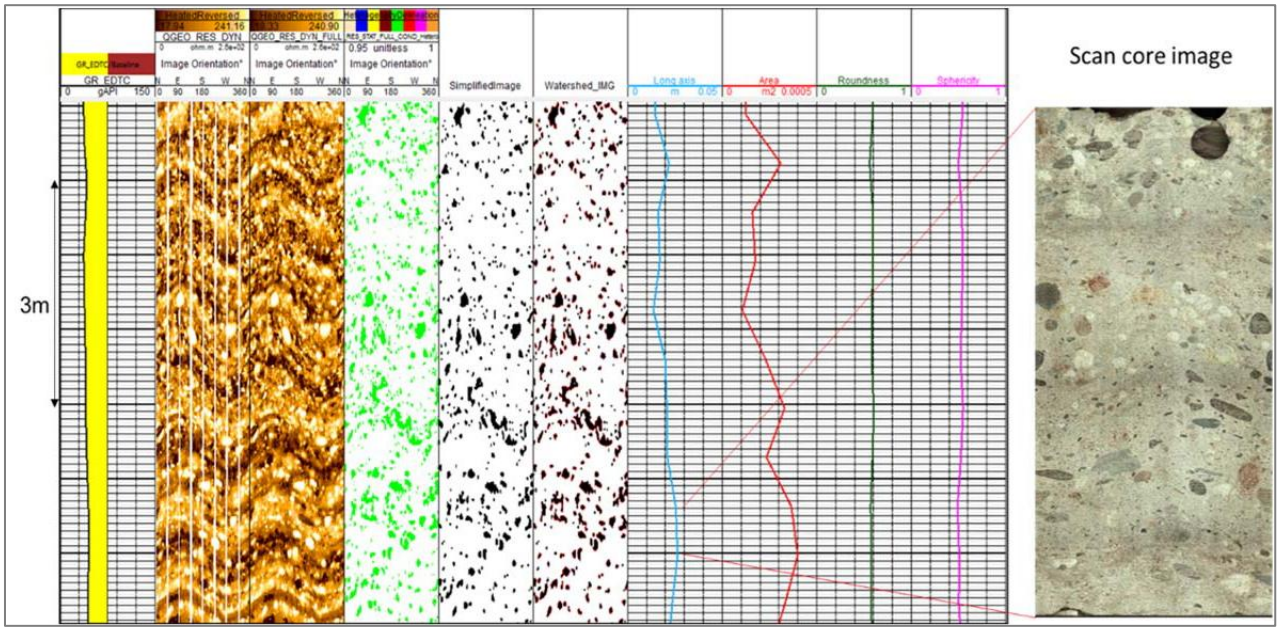

Figure 7. Particle shape analysis verified with core scan image. The tracks are same as in Figure 5.

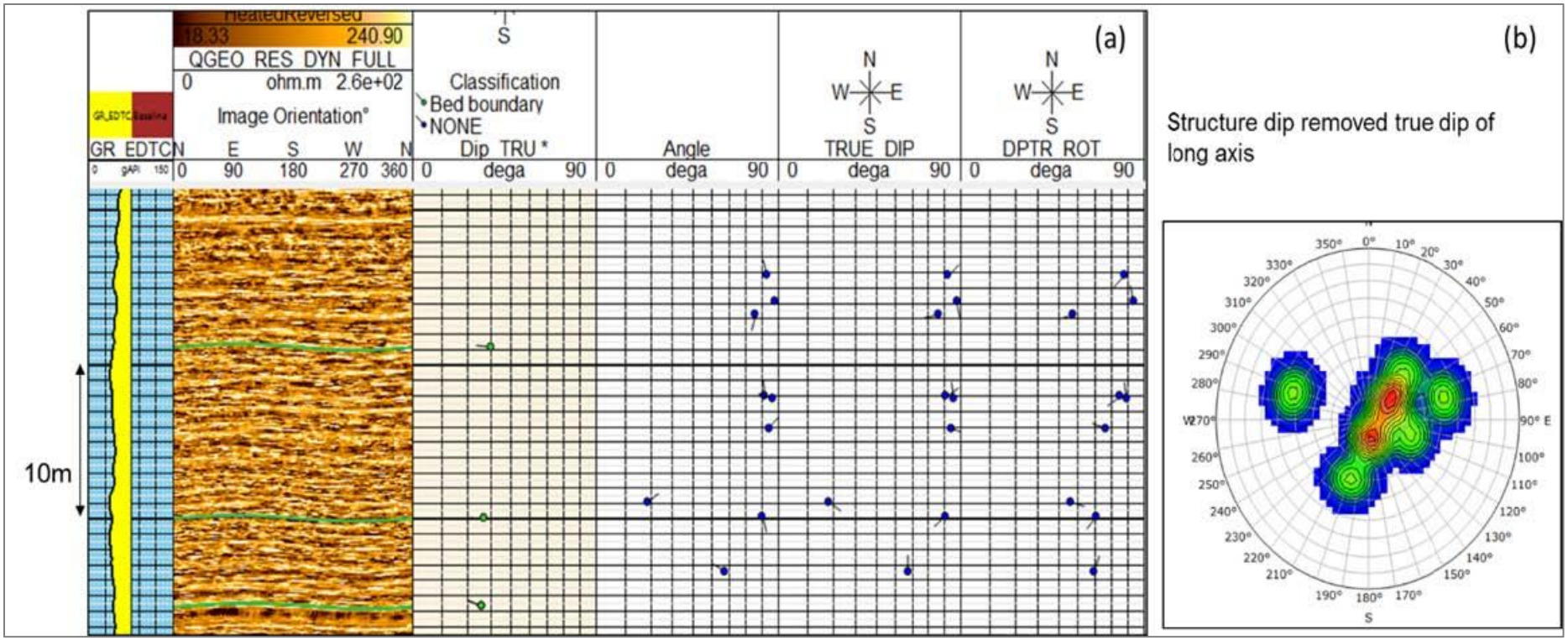

Figure 8. Long axis dip process and display in stereonet. (a) Track 1, gamma ray with baseline display; track 2, gap filled dynamic borehole resistivity image; track 3, bedding boundary dips; track 4, apparent dips of long axis; track 5, true dip of long axis; track 6, structure removed true dip of long axis. (b) Structure dip removed true line dip display in stereonet.

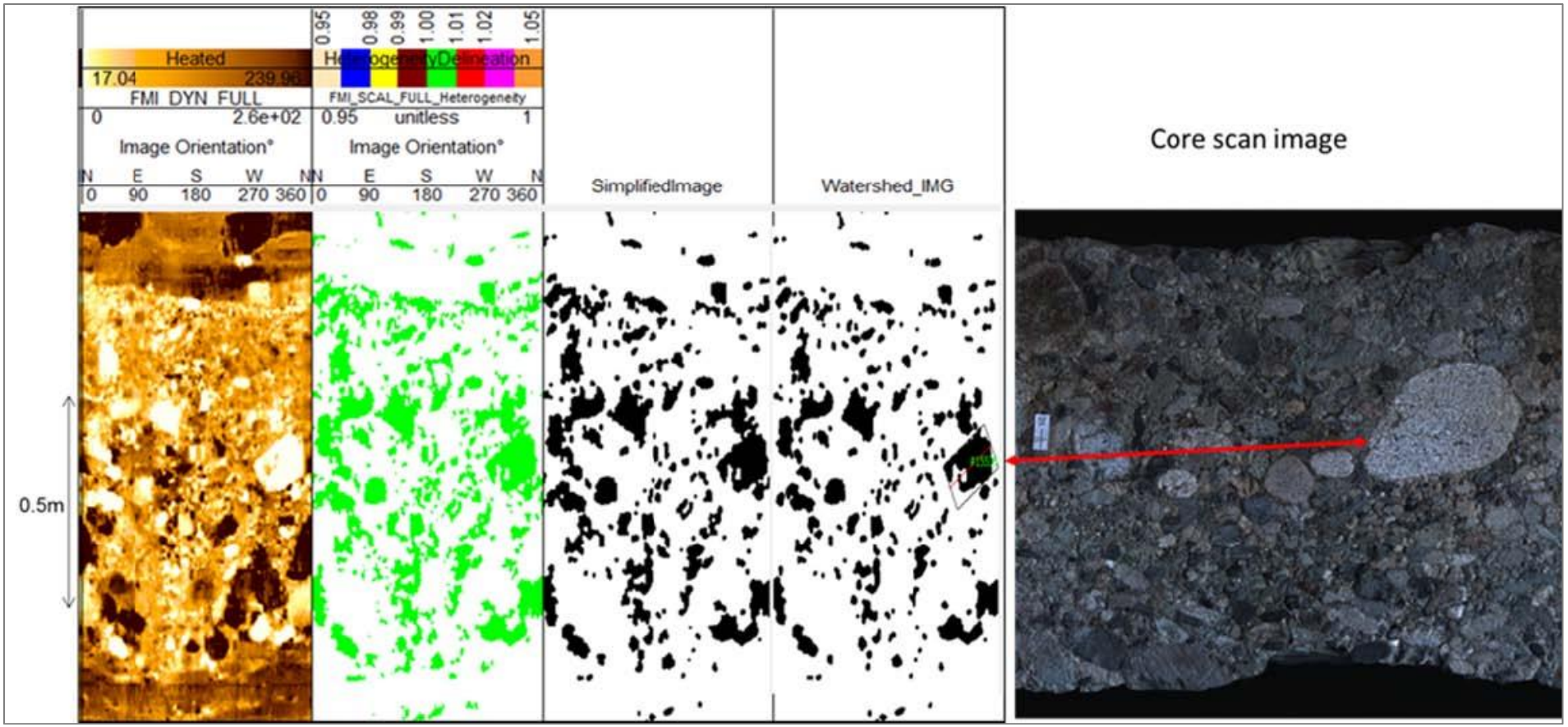

Figure 9. Particle shape analysis with core image calibration. Track1, gap-filled dynamic borehole resistivity image; track 2, extracted resistivity patches; track 3, simplified resistivity patches; track 4, separated resistivity patches from watershed transform; track 5, core scan image.

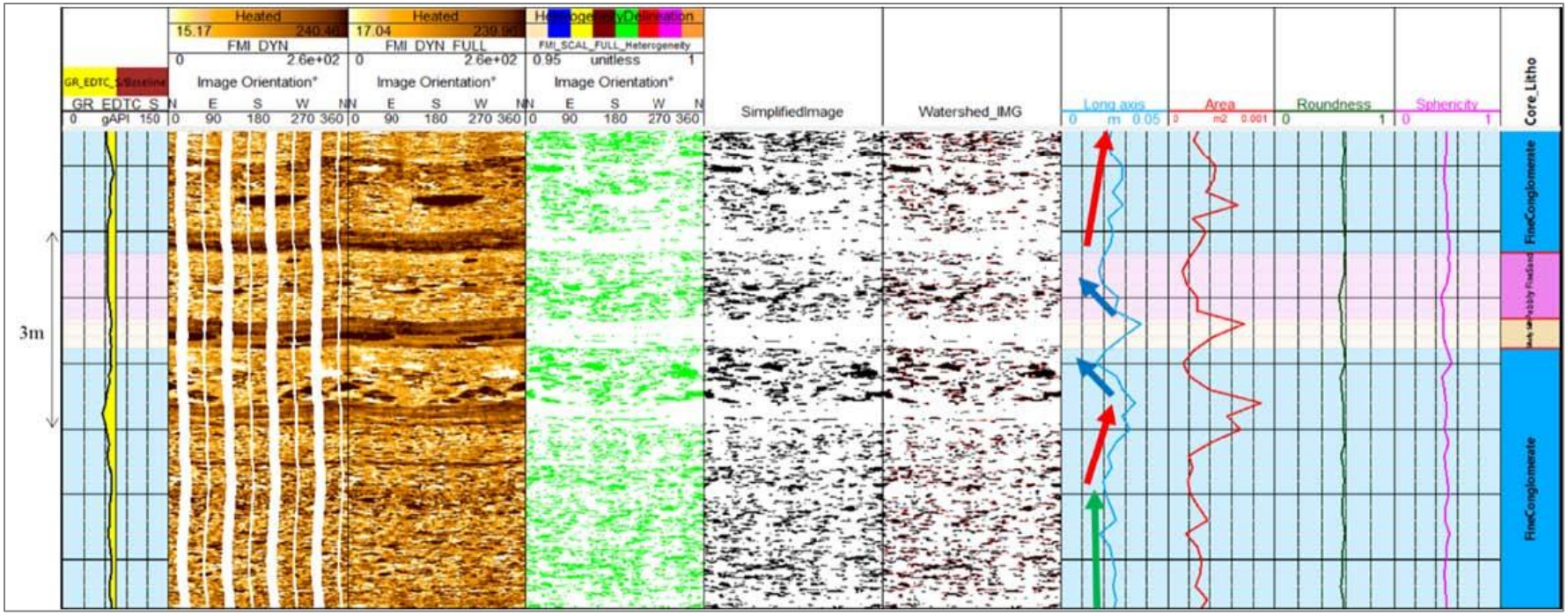

Figure 10. Particle shape analysis middle and final results. The tracks are the same as in Figure 5.

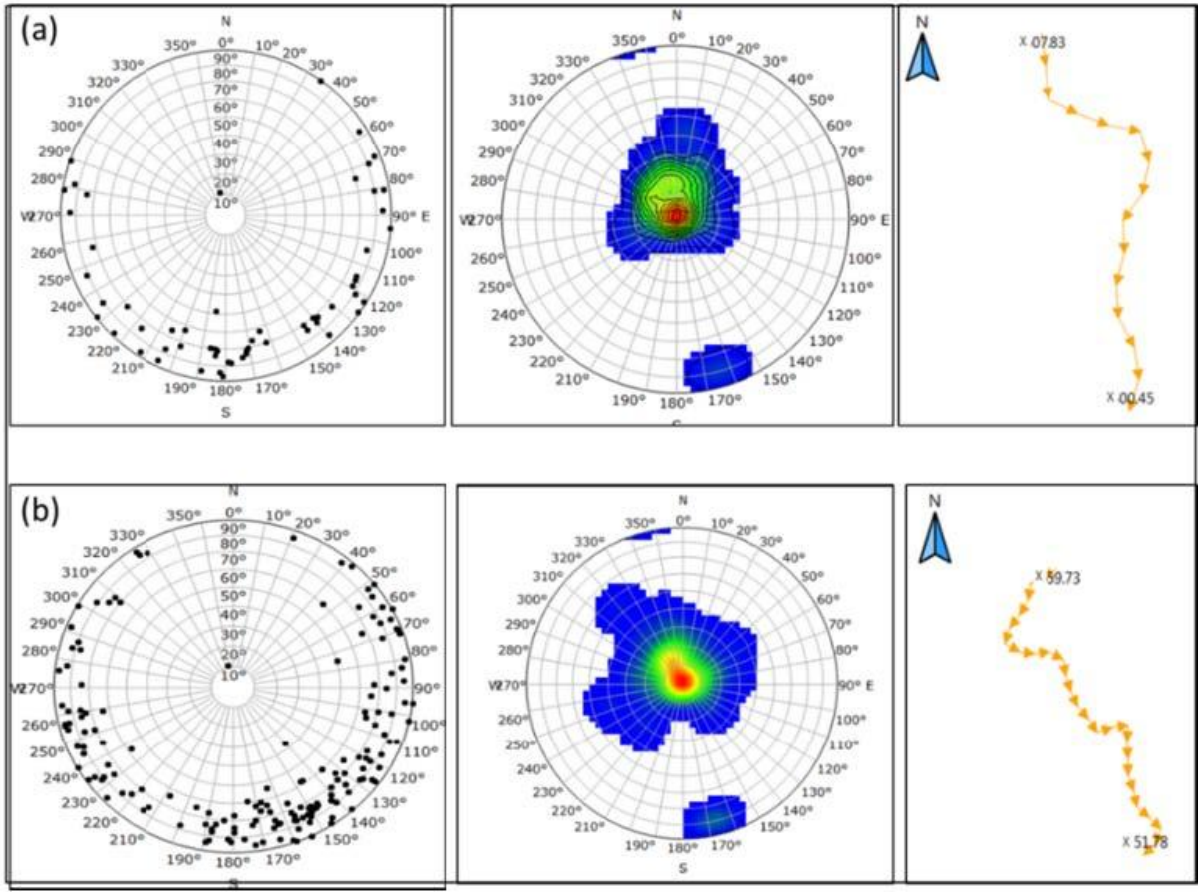

Figure 11. Paleocurrent analysis from the long-axis direction display in stereonet and dip vector plot with crossbedding. The first stereonet plot (left) is long-axis true dip displayed as the pole of planar dip. The second stereonet plot (middle) is the same long-axis dips displayed as line dip with density and contour. The third plot (right) is dip vector plot with structure dip removed crossbedding dips.

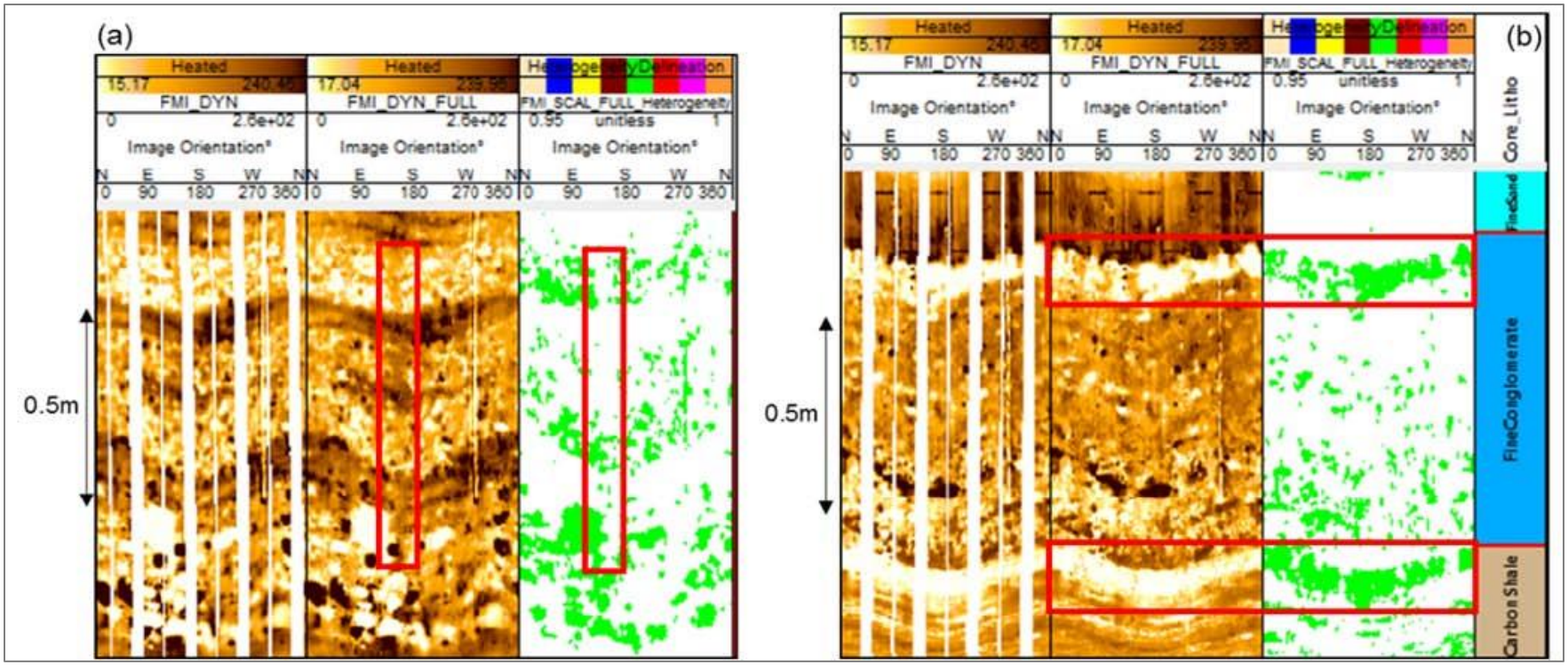

Figure 12. (a) Reconstructed borehole image with vertical stripe; (b) extracted resistivity patches from carbonate shale and diagenesis feature.